Acta Crystallographica Section B
Structural Science
ISSN 0108-7681

Neutron powder diffraction refinement of $PbZr_{1-x}Ti_xO_3$

N. Zhang,[a] H. Yokota,[a]* A. M. Glazer[a] and P. A. Thomas[b]

[a]Clarendon Laboratory, Department of Physics, University of Oxford, England, and [b]Department of Physics, University of Warwick, England

Correspondence e-mail: yokota@physics.s.chiba-u.ac.jp

Received 4 May 2011
Accepted 16 July 2011

Rietveld refinement of different structural models using neutron diffraction data for a series of powders of lead zirconate titanate, $PbZr_{1-x}Ti_xO_3$ (PZT), is described. It is found that at all the compositions and temperatures studied the best results include contributions from more than one phase in order to fit the data. Consequently a new phase diagram is proposed.

1. Introduction

Lead zirconate titanate, $PbZr_{1-x}Ti_xO_3$ (PZT-x), is a solid solution of ferroelectric lead titanate, $PbTiO_3$, and antiferroelectric $PbZrO_3$ (Sawaguchi, 1953). The phase diagram of PZT proposed by Jaffe *et al.* (1971) was largely accepted for many years. At a Ti concentration of approximately 48% there is an almost vertical line known as the morphotropic phase boundary (MPB) separating Ti-rich tetragonal and Zr-rich rhombohedral phases. Near the MPB many physical properties, such as piezoelectricity, dielectric constant and electromechanical constant, are increased to a maximum.

In the Zr-rich region the crystal structure of PZT has long been regarded as having two ferroelectric rhombohedral phases, $R3c$ (F_{LT}) at room temperature and $R3m$ (F_{HT}) at higher temperature. In the F_{LT} phase there are, in addition, antiphase oxygen octahedral tilts denoted by $a^-a^-a^-$ (Glazer, 1972), which decrease in magnitude and become zero in the F_{HT} phase with the tilt system $a^0a^0a^0$. The existence of oxygen octahedral tilts in F_{LT} leads to a doubled pseudo-cubic unit cell of $\sim 8 \times 8 \times 8$ Å^3. On the Ti-rich side of the phase diagram the structure is tetragonal in space group $P4mm$ with cation displacements along the $[001]_{pc}$ direction, where the subscript 'pc' denotes the single pseudo-cubic perovskite unit cell.

Structural studies around the MPB region have been published by a number of authors. Some observed that the Pb atom showed a flattening of the probability ellipsoid calculated from its anisotropic displacement parameters (ADPs) to form a disk perpendicular to the polar axis (Glazer *et al.*, 1978; Corker *et al.*, 1998), which was explained by disordered Pb displacements slightly off the polar axis so that locally at the unit cell level the structure was in fact monoclinic (Corker *et al.*, 1998). An intermediate monoclinic phase was subsequently found by Noheda *et al.* (1999) whose space group (Cm) is a subgroup of both $R3c$ ($R3m$) and $P4mm$, and thus can act as a 'bridging' phase. This pioneering work has encouraged a large number of structural studies especially around the MPB. Several models including Cm, Cc, Pc, $F1$ space groups and different combinations of mixed structures have been proposed using different experimental methods (Pandey *et al.*, 2008; Liu *et al.*, 2001; Fraysse *et al.*, 2008; Ragini *et al.*, 2002). The importance of the monoclinic phase is that it

suggests a mechanism for the high piezoactivity near the MPB, since it allows for the Pb displacements to rotate within a mirror plane on applying a stress or electric field, the so-called polarization rotation model (Noheda *et al.*, 2001). However, the existence of the monoclinic phase has been questioned in favour of an adaptive phase model (Jin *et al.*, 2003; Wang, 2006, 2007) that gives rise to apparent extra diffracted intensity caused by domain-wall scattering and which might be mistaken for the presence of a monoclinic phase. This model also suggests a mechanism for piezoactivity through the movement of domain walls under an applied stress of electric field. Thus, determination of the precise nature and symmetry of the crystal structure of PZT is important if this disagreement is to be resolved.

With respect to the Zr-rich PZT region we previously carried out a series of high-resolution time-of-flight neutron diffraction experiments for $0.08 < x < 0.40$ at 300 K and found that the best fits by the Rietveld method were obtained with mixed phases of rhombohedral *R*3*c* and monoclinic *Cm* symmetry (Yokota *et al.*, 2009). The *Cm* fraction was found to increase towards the MPB; this mixed-phase model explains why no actual boundary has been observed between rhombohedral and monoclinic phases in experiments to date.

On the Ti-rich side, it has been determined that the symmetry is tetragonal, *P*4*mm*. However, Raman experiments at low temperature suggested a phase transition from tetragonal to monoclinic *via* an intermediate orthorhombic phase for $0.5 < x < 0.6$ (Frantti *et al.*, 1999). Therefore, even in the Ti-rich region there are still ambiguities about the crystal structure of this material.

Above the Curie temperature, Kuroiwa *et al.* (2005) carried out high-energy synchrotron-radiation powder diffraction experiments. They noted that there was a systematic discrepancy in the profile fits for different reflections and this was explained by making the Pb atoms disordered and displaced from their high-symmetry positions in the ideal cubic structure. In their model the Pb atoms are shifted along $\langle 111 \rangle_{pc}$ directions for Zr-rich PZT and along $\langle 110 \rangle_{pc}$ directions for Ti-rich compositions.

The difficulty in determining the precise symmetry has been caused by the lack of single crystals until very recently, and as a result most structural refinements have been carried out with powder or ceramics. Additionally, many of the proposed models provided similar *R* factors and calculated profiles. Very recently, Bokov *et al.* (2010) succeeded in growing single crystals whose concentrations are around the MPB by top-seeded methods, but so far they are not of sufficient quality to enable unambiguous structure determination to be made. It is worth mentioning here that earlier Pandey *et al.* (2008) suggested that the rhombohedral phases in fact were monoclinic, space groups *Cc* (instead of *R*3*c*) and *Cm* (instead of *R*3*m*). This is an attractive idea since it explains the lack of a boundary on the rhombohedral side and also suggests that the observed flat ADP ellipsoids are a consequence of refining the structure in too high a symmetry. However, the only way to prove this idea is to search for the presence of an additional peak at a *d*-spacing of ~ 4.7 Å, which is expected in the space group *Cc*. X-ray powder diffraction had so far failed to find this peak and recently a neutron diffraction study of single-crystal PZT found no evidence for this reflection (Phelan *et al.*, 2010). Furthermore, the neutron diffraction experiments suggested that even in the crystal there is coexistence of phases with symmetries *R*3*c* and *Cm*. More recently Gorfman *et al.* (2011) carried out high-resolution X-ray diffraction experiments on crystals with $x \simeq 0.31$ and 0.45 and have shown the presence of mixed phases of rhombohedral and monoclinic symmetries.

This work has led us to undertake more precise structural refinements through the MPB region. In the present paper, time-of-flight neutron diffraction using PZT ceramics with $0.3 \leq x \leq 0.6$ at several temperatures is described. It has been found that the monoclinic phase exists over the whole region below the Curie temperature. Around the MPB, the structure becomes more complicated and we suggest that it is the large number of interfaces between these different phases that is the main reason for the enhancement of the extrinsic component of the observed piezoelectricity.

2. Experiments

Ceramic samples were prepared by the conventional mixed oxide method. Details of sample preparation conditions can be found in the paper by Yokota *et al.* (2009). All the samples were checked at 300 K for the presence of secondary phases and their quality was checked by X-ray diffraction using a Panalytical X'PERT powder diffractometer fitted with an incident-beam Johannssen-cut focusing monochromator to isolate the Cu $K\alpha_1$ line.

The neutron powder diffraction measurements were performed at ISIS (Rutherford–Appleton Laboratory) on the HRPD (high-resolution powder diffractometer). The samples were packed in vanadium canisters with a diameter of 12 mm for both room-temperature and high-temperature experiments. For the low-temperature experiments the sample was packed into a rectangular vanadium container covered with a cadmium plate. To eliminate scattering from the cadmium plate, gadolinium foil was used as a shield. A vacuum furnace with vanadium heating element and a cryostat were used for the high- and low-temperature measurements. The data collection at 300 K was carried out without a furnace or cryostat. The exposure time for each measurement was around 2.5 h. PZT-*x* samples with $x = 0.3$, 0.4, 0.45, 0.48, 0.5, 0.6 were measured at a series of temperatures from 8 to 623 K.

3. Results

Rietveld refinement was carried out using *TOPAS Academic* (Coelho, 2005). The data were collected using the high-angle back-scattering bank detectors, which provide the *d*-spacing range ~ 0.3–2.2 Å. Since the disk-shaped ADP ellipsoids for the Pb atoms in PZT are to some extent an artifact caused by using a limited *d*-spacing range (Corker *et al.*, 1998), it is necessary to use as full a *d*-spacing range as possible for refinement (Yokota *et al.*, 2009). Several different structural

Table 1
Freely refineable structural parameters for the space group models used in the refinement of the PZT system.

Space group	Lattice vectors	Ion	Wyckoff	x	y	z	Tilt system
*P*4*mm*	$a_t = a_{pc}$, $c_t = c_{pc}$	Pb	4*d*	$\frac{1}{2}$	$\frac{1}{2}$	$\frac{1}{2} + \delta z_{Pb}$	$a^0a^0a^0$
		Zr/Ti	1*b*	0	0	0	
		O1	1*b*	0	0	$\frac{1}{2} + \delta z_{O1}$	
		O2	2*c*	$\frac{1}{2}$	0	δz_{O2}	
Cm	$a_m = a_{pc} + b_{pc}$, $b_m = b_{pc} - a_{pc}$, $c_m = c_{pc}$	Pb	2*a*	0	0	0	$a^0a^0a^0$
		Zr/Ti	2*a*	$\frac{1}{2} + \delta x_{Zr/Ti}$	0	$\frac{1}{2} + \delta z_{Zr/Ti}$	
		O1	2*a*	$\frac{1}{2} + \delta x_{O1}$	0	δz_{O1}	
		O2	4*b*	$\frac{1}{4} + \delta x_{O2}$	$\frac{1}{4} + \delta y_{O2}$	$\frac{1}{4} + \delta z_{O2}$	
Cc	$a_m = a_{pc} + b_{pc} + 2c_{pc}$, $b_m = a_{pc} - b_{pc}$, $c_m = a_{pc} + b_{pc}$	Pb	4*a*	0	$\frac{3}{4}$	0	$a^-a^-a^-$
		Zr/Ti	4*a*	$\frac{1}{4} + \delta x_{Zr/Ti}$	$\frac{1}{4}$	$\frac{1}{4} + \delta z_{Zr/Ti}$	
		O1	4*a*	δx_{O1}	$\frac{1}{4}$	δz_{O1}	
		O2	4*a*	$\frac{1}{4} + \delta x_{O2}$	$\frac{1}{2} + \delta y_{O2}$	δz_{O2}	
		O3	4*a*	$\frac{1}{4} + \delta x_{O3}$	δy_{O3}	$\frac{1}{2} + \delta z_{O3}$	
*R*3*c*†/*R*3*m*	$a_h = b_{pc} - a_{pc}$, $b_h = c_{pc} - b_{pc}$, $c_h = a_{pc} + b_{pc} + c_{pc}$	Pb	6*a*	0	0	$s + \frac{1}{4}$	$a^-a^-c^-/a^0a^0a^0$
		Zr/Ti	6*a*	0	0	T	
		O	18*b*	$\frac{1}{6} - 2e - 2d$	$\frac{1}{3} - 4d$	$\frac{1}{12}$	
*I*4*cm*‡	$a_t = a_{pc} + b_{pc}$, $b_t = b_{pc} - a_{pc}$, $c_t = 2c_{pc}$	Pb	4*b*	0	$\frac{1}{2}$	$\frac{1}{4} + \delta z_{Pb}$	$a^0a^0c^-$
		Zr/Ti	4*a*	0	0	0	
		O1	4*a*	0	0	$\frac{1}{4} + \delta z_{O1}$	
		O2	8*c*	$\frac{1}{4} + f$	$\frac{3}{4} + f$	δz_{O2}	

† In the rhombohedral system the unit cell used is with reference to the hexagonal setting (Megaw & Darlington, 1975). The parameters s and t are the fractional cation displacements along the polar axis; d is the octahedral distortion keeping triad-axis symmetry, but making the upper and lower faces different in size; e describes the octahedron rotation about the triad axis. This *R*3*c* symmetry has also been used to describe the *R*3*m* phase by setting $e = 0$. ‡ The parameter f is a measure of the oxygen octahedral tilt.

models were tried for different compositions and temperatures, including single and mixed phases. Mixtures showed much better fits for most of the data, especially in the MPB region. A detailed comparison will be discussed in the following sections.

Several TEM experiments have suggested nano-domain structures around the MPB (Asada & Koyama, 2004, 2007; Theissmann *et al.*, 2007) and it is known that the scattering experiments are faced with difficulties in analyzing the data from samples with small domains and strains because of coherence effects that lead to peak broadening (Boysen, 2007). Boysen (2005) claimed that the domain structure causes anisotropic broadening of reflections and asymmetries in the diffraction pattern of $PbTiO_3$, and this could lead to an incorrect structural model being used for Rietveld refinement. Therefore, we incorporated into our refinements the anisotropic line-shape broadening function proposed by Stephens (1999). Since nano-domains are found in particular in and around the MPB, such effects are likely to be more prevalent in this region. This tendency was found during the refinement process. The scale factor, background parameters, peak-shape function parameters and absorption parameters were refined in all cases. In order to minimize the refined parameters, isotropic displacement displacements were used for the Zr/Ti atoms and all the other atoms when the anisotropic peak-broadening function was applied. Bond valences were also calculated to examine the crystal structures, and thermal correction was applied to these for the low- and high-temperature runs (Frantti *et al.*, 2002; Brown, 2002). The corrected bond valences for Pb, Zr/Ti and O ions have been found to be around 1.8–2.0, 3.8–4.0 and 1.9–2.0. Table 1 lists the refineable structural parameters for each possible space group (note that in the rhombohedral *R*3*c* refinements the unit cell axes were chosen with respect to the hexagonal setting and the parameters refined were those described by Megaw & Darlington, 1975). The final values of R_{wp} for each model are summarized in Table 2.[1]

3.1. Ti-rich region (x = 0.6)

The boundary between monoclinic and tetragonal phases has been well defined for a long time and in general Ti-rich PZT has been considered to be a single tetragonal phase. Therefore, a single *P*4*mm* model was examined for PZT-0.6 below the Curie temperature. The refinement procedure worked smoothly but the refinement results produced rather large agreement factors. We found that the intensities of some reflections did not fit well and were underestimated even when strain was taken into account. The only exception was PZT-0.6 at 573 K, which fitted quite well for a single *P*4*mm* model, but with strain included.

For data that could not be fully explained by the single-phase *P*4*mm* model, a mixed model consisting of *P*4*mm* and *Cm* was tried, and the refinement results showed a significant improvement. Refinement of the relative phase percentages suggested that there was around 50–60% of the *P*4*mm* phase present. On increasing the temperature the amount of the *P*4*mm* phase appeared to increase, with the sample becoming single phase just below the Curie temperature. The difference in lattice constants a and c was found to become smaller on heating as the cubic phase is approached, as expected.

First-principles calculations by Kornev *et al.* (2006) suggested that PZT at low temperature with $0.475 < x < 0.51$ is in space group *Cc* and that for $0.51 < x < 0.56$ it is *I*4*cm*. In these space groups tilting of the octahedra would be expected.

[1] Supplementary data for this paper are available from the IUCr electronic archives (Reference: KD5052). Services for accessing these data are described at the back of the journal.

Table 2
Values of weighted profile R_{wp} for different models.

Best fits marked in bold. Asterisks denote where strain refinement is included (* indicates strain was applied for the first phase in the title of the column; † indicates the second phase; ‡ indicates the third phase).

x	T (K)	*R3c*	*Cm*	*P4mm*	*Cc*	*R3c* + *Cm*	*P4mm* + *Cm*	*P4mm* + *Cm* + *R3c*	*Cc* + *Cm*	*F*1	*I4cm*	*I4cm* + *Cm*
0.6	10			*3.61			***2.63**				*3.81	*†2.97
	300			*5.13			***3.50**					
	473			***2.98**								
0.5	10		*6.92		*8.51		*†5.58	*†‡**3.64**	*†5.67			
	300		*8.36	*9.25		*†6.40	*†3.91	*†**3.42**				
	473		*3.73	*4.15			***†2.52**					
0.48	13		*6.39		*9.06	*†4.24		†‡**3.61**	*†5.80	9.06		
	300		*7.88	*11.25		*†4.71	*†4.45	*†‡**3.55**				
	473		*4.75	*4.59			***†2.53**					
	623		*3.65	*3.21			***2.30**					
0.45	10	*9.04	*7.24		*7.19	*†3.55		†‡**3.10**				
	200	*5.96	*5.76			***†3.04**						
	300	*5.39	*5.28			***†4.06**						
	473	*7.46	*5.05	*6.13		*†4.57		**†3.15**				
	623		*3.34	*2.53			***2.13**					
0.4	10	*4.02				***2.84**						
	300	*5.37				***3.15**						
	473	*2.99				***†2.73**						
	573					***†3.12**	†2.88					
0.3	8	*3.94				***2.97**						
	200	*4.32				***3.06**						
	300	*5.44				***3.87**						

Kornev *et al.* (2006) proposed a mixed model containing *I4cm* + *Cc* phases for x = 0.51 because of the likelihood of compositional fluctuations in the sample. As the composition for this sample (x = 0.6) is close to the compositions Kornev *et al.* (2006) proposed for the *I4cm* phase, we refined this model including strain parameters using the 10 K data. This gave a higher R_{wp} value than a single *P4mm* model, and the mixed model containing *I4cm* + *Cm* phases did not work as well as a mixture of *P4mm* + *Cm*. Fig. 1 shows some fitted profiles for PZT-0.6 measured at 10 K for these three models mentioned above. Note too (for example see Fig. 2) that no peaks indicating tilted octahedra were observed, and therefore we find no evidence for an *I4cm* phase.

3.2. Zr-rich region (x = 0.3, 0.4)

For Zr-rich concentrations, a single rhombohedral model had generally been accepted below the Curie temperature. Recently, however, a mixed *R3c*/*R3m* + *Cm* model was proposed at 300 K for these compositions (Yokota *et al.*, 2009) and so it was important to examine this model at different temperatures.

Both single *R3c* and a mixture of *R3c* + *Cm* models were tried for these two compositions from low to high temperature, and the mixed-phase models gave a better fit than the single-phase models for all the temperatures, which confirms the previous results (Yokota *et al.*, 2009; see Fig. 3). As some reflections showed obvious broadening in the observed data, *R3c* strain parameters were included for PZT-0.3, and both *R3c* and *Cm* strain effects were introduced for PZT-0.4 because of the increase of the *Cm* fraction with higher x. It was found that the refinements showed that with increasing temperature the *R3c* phase fraction decreases while the *Cm* fraction increases. For PZT-0.4, at 10 K, *R3c* is the major phase accounting for around 70%. From 473 K it becomes less than 50% and decreases still more at higher temperature [49 (2)% at 473 K, 46 (2)% at 553 K, 38 (2)%

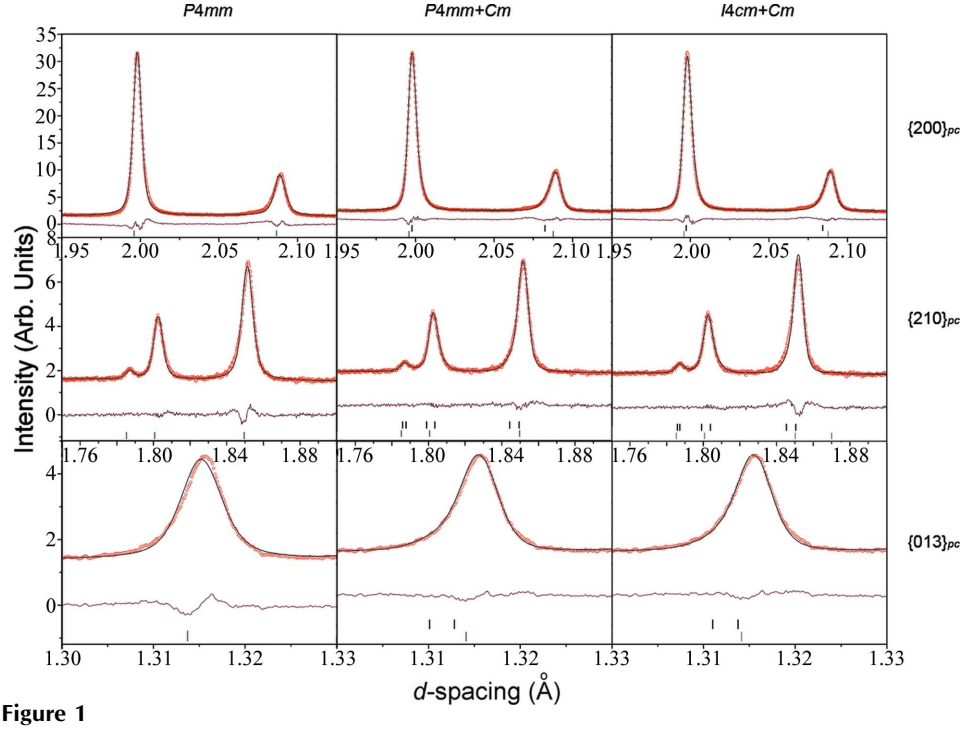

Figure 1
Refined profiles of PZT-0.6 at 10 K. Experimental data: red; calculated fit: black line. Ticks below: *Cm* reflections – black; *P4mm* reflections – green; *I4cm* reflections – red. Results for $\{200\}_{pc}$, $\{210\}_{pc}$ and $\{013\}_{pc}$ reflections are shown. This figure is in colour in the electronic version of this paper.

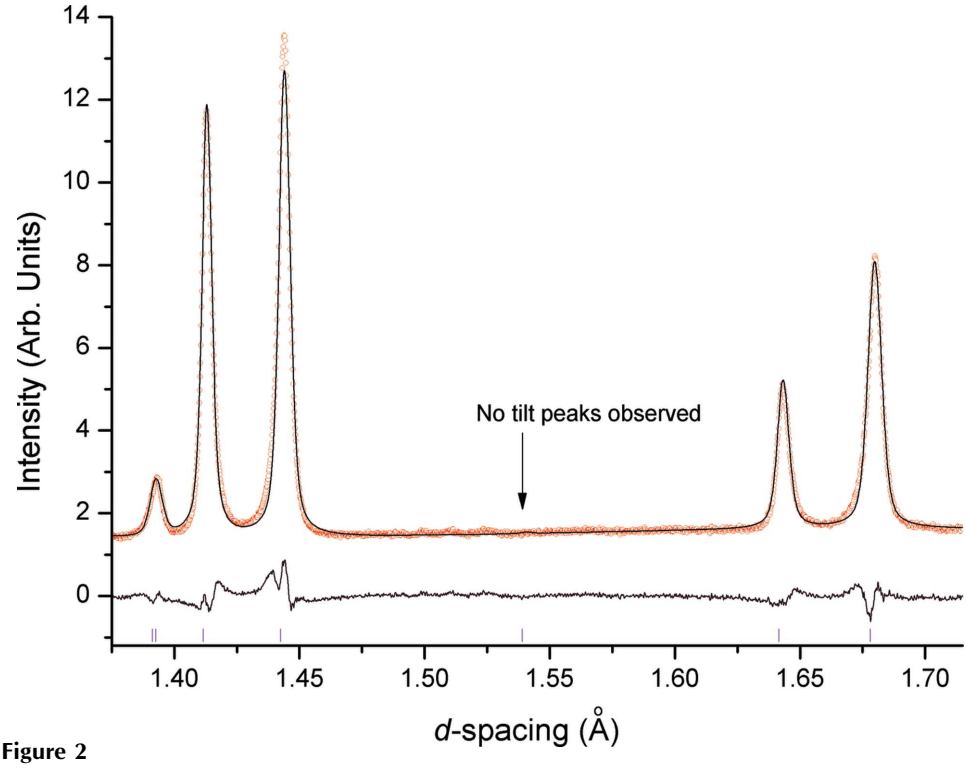

Figure 2
Some observed profiles of PZT-0.6 at 10 K. The black arrow points to the position where tilt peaks might be expected for a structure in space group *I*4*cm*.

at 573 K and 31 (2)% at 593 K]. The *R*3*c* fractions for PZT-0.3 are 80.9 (4), 70.0 (6) and 60.8 (8)% at temperatures of 8, 200 and 300 K.

Around 573 K the overall PZT-0.4 powder profile was fitted with a model consisting of *Cm* + *P*4*mm* as well as for a mixture of *R*3*m* + *Cm*. At 553 and 573 K, the pattern shows that the $\{222\}_{pc}$ peak displays a shoulder on the high *d*-spacing side, indicating splitting of this reflection, which can be caused by the presence of the *R*3*m* phase, and on approaching 593 K the split gradually disappears to form a single peak. This indicates either a decrease in the amount of *R*3*m* or a structural change. The calculated pseudocubic lattice parameters at 573 K for the *R*3*m* phase are a_{pc} = 4.0918 (4) Å, α_{pc} = 89.899 (2)°, and for the *P*4*mm* phase *a* = 4.0888 (2), *c* = 4.0968 (6) Å. Both are very close to that expected for the cubic phase, and so around this temperature the *R*3*m* and *P*4*mm* structures are too similar to be reliably distinguished. This suggests that the different phases around this region are energetically equivalent and so this must be close to the transition

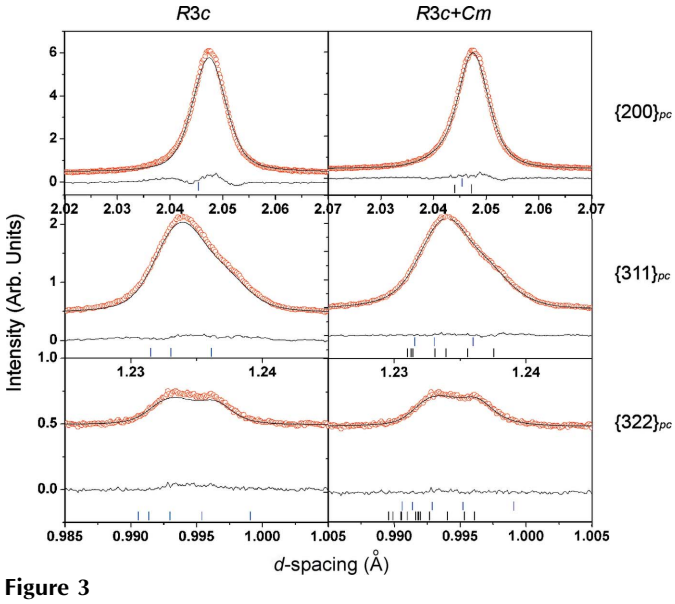

Figure 3
Refined profiles of PZT-0.4 at 473 K. The blue small ticks correspond to *R*3*c* reflections and the black ticks to *Cm*. The refinement results of single *R*3*c* with strain are shown at the left and *R*3*c* + *Cm* model at the right. This figure is in colour in the electronic version of this paper.

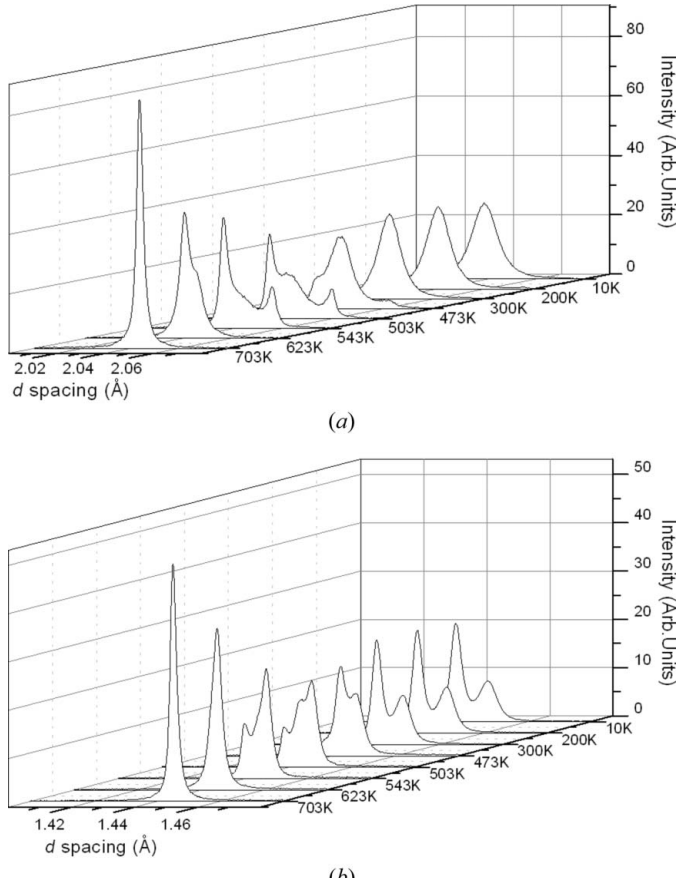

Figure 4
Three-dimensional plot of (*a*) $\{200\}_{pc}$ and (*b*) $\{220\}_{pc}$ profiles for PZT-0.45 at various temperatures.

boundary between low-temperature and cubic phases and the boundary between the Zr-rich and the MPB phases, where a tricritical point is known to exist (Ye *et al.*, 2010).

3.3. The MPB region (x = 0.45, 0.48, 0.50)

A series of $\{200\}_{pc}$ profile plots at different temperatures from 10 to 703 K for PZT-0.45 is shown in Fig. 4(*a*). A clear increase in the splitting of peaks is observed around 503 K, which is consistent with the appearance of a tetragonal phase. The intensity of these tetragonal peaks continues to increase with temperature while at the same time the rhombohedral peak in the middle decreases: the two phases coexist for a wide temperature range. The phase change at this temperature can be confirmed with the $\{220\}_{pc}$ profile plot (Fig. 4*b*). Mixed *R*3*c* + *P*4*mm* models were tried for the 473 and 503 K data, but the discrepancy between the observed and calculated intensities was large. Generally this two-phase model cannot explain many of the complicated peak shapes, and so we introduced *Cm* into this model and the fit was significantly improved (R_{wp} dropped from 0.040 to 0.024).

From the peak pattern it is clear that the major phase at temperatures lower than this phase coexistence area is rhombohedral while at higher temperature it is tetragonal. We used *R*3*c* + *Cm* at 200 and 300 K, *P*4*mm* + *Cm* at 543 and 623 K because they all gave much better fits than any single-phase models. At 10 K the broadening of the $\{200\}_{pc}$ peak is much larger than at 200 and 300 K, and cannot be explained by the *R*3*c* + *Cm* model. A mixture of *R*3*c* + *Cm* + *P*4*mm* was used and this model is consistent with the low-temperature phases of the MPB region (PZT-0.48 and PZT-0.5), which will be discussed below.

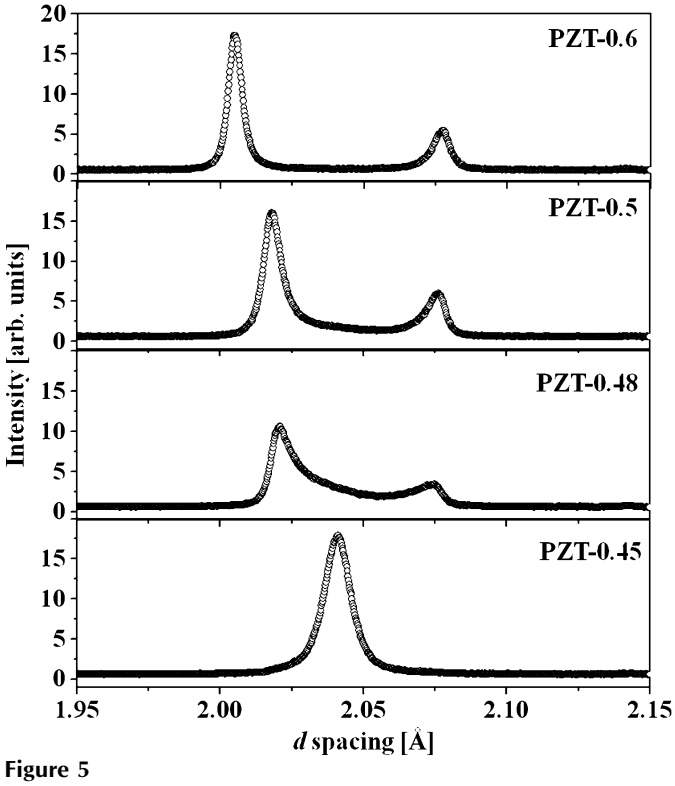

Figure 5
Changes in $\{200\}_{pc}$ reflection profiles of PZT-0.60, 0.50, 0.48 and 0.45 at room temperature.

For PZT-0.48 and PZT-0.50 at room temperature and at low temperatures, several papers have considered this region to be single phase, either tetragonal *P*4*mm* or monoclinic *Cm* or *Cc*, or even triclinic *F*1 (Liu *et al.*, 2001; Fraysse *et al.*, 2008). Fig. 5 shows the change of the $\{200\}_{pc}$ reflections as a function of Ti concentration at 300 K. For the Zr-rich side with $x \leq 0.45$, this reflection appears to be a single peak whose FWHM becomes broad with increasing x. On increasing the Ti concentration through the MPB ($x \geq 0.48$), the $\{200\}_{pc}$ reflection starts to split into two main peaks with long tails and relatively large FWHMs. This peak shape cannot be accounted for by a single phase even if the effect of strain is taken into account and the poor R_{wp} values for the refinements of the single-phase models (Table 2) support this conclusion. Attempts at fitting the data using a *P*4*mm* phase including local disordered ⟨110⟩ Pb displacements (Noheda *et al.*, 2000) were also unsuccessful.

Regarding the unusually broad and asymmetric peak shapes for PZT-0.48 and PZT-0.5 at low temperature and at 300 K (Figs. 6–9), it is probable that in this region there is a coexistence of several different phases. Ragini *et al.* (2002) performed X-ray diffraction and Rietveld analysis for $0.515 < x < 0.530$ at room temperature, and they claimed that the high-temperature tetragonal *P*4*mm* and the low-temperature *Cm* phases coexist as a result of the occurrence of a first-order phase transition. We also found that refinement using this mixed-phase model was much better than for the single-phase models. However, the observed and fitted profiles were still not quite in agreement. A mixture of *R*3*c* + *Cm* was also tried for PZT-0.48, but this also turned out to be unsuccessful. At low temperature a two-phase mixture of *Cc* + *Cm*, as suggested by Cox *et al.* (2005), was refined but this model did not help to fit the $\{200\}_{pc}$ reflections. Finally, a three-phase mixture of *R*3*c* + *Cm* + *P*4*mm* with strain parameters included was tried for these compounds. Figs. 6–9 show part of the refined profiles for PZT-0.48 and PZT-0.5 at around 10 and 300 K, respectively. This refinement improved the fit significantly. In particular, tails observed next to the main peaks (*i.e.* $\{200\}_{pc}$, $\{311\}_{pc}$ reflections) were reproduced with this model. When the strain terms were not included in the refinement the characteristic tails and shoulders observed in these profiles were not reproduced. Addition of a cubic structure as proposed by Noheda *et al.* (2000) did improve the strain-free model: however, the existence of the cubic phase so far below the Curie temperature seems unlikely, and so we decided against using a four-phase mixture. Our refinement results indicate that the strain becomes more significant on approaching the MPB.

As mentioned before, the PZT-0.45 data measured at 10 K were also refined best with this three-phase mixture model, but the proportion for each phase was found to have changed. The *R*3*c* component decreases rapidly on approaching the MPB [72.3 (7)% for PZT-0.45 at 10 K and 30.2 (6)% for PZT-0.48 at 13 K] and becomes a minor phase for PZT-0.5 [19.4 (4)% at 10 K and 8.5 (4)% at 300 K]. The fraction of the

Cm phase increases in the MPB region and reaches its maximum value of 65.9 (6)% when x = 0.5, T = 10 K. The amount of *P*4*mm* phase increases with a further increase in the Ti composition.

The powder patterns for PZT-0.45, PZT-0.48 and PZT-0.5 at 473 K or higher appeared to be less complicated than at lower temperatures. However, the long tails still exist in many main reflections. Single *P*4*mm* and *Cm* models were tried with strain included but neither of them was able to fit the saddle points between two separated reflections such as $\{002\}_{pc}$ and $\{200\}_{pc}$ (Fig. 10). The refined lattice parameters of PZT-0.48 at 473 K for the *Cm* phase were a = 5.7343 (2), b = 5.7305 (2), c = 4.11804 (4) Å, and β = 90.081 (2)°. The difference between a and b was only 0.06% and so the unit cell of the *Cm* phase was metrically almost consistent with a tetragonal crystal system. This provides a possible explanation for the powder pattern having as its major phase tetragonal *P*4*mm* with a small amount of another phase. Therefore, refinement with a mixed *P*4*mm* + *Cm* model was performed; the same model that was applied to Ti-rich PZT. Fig. 10 depicts part of the refinement profiles of PZT-0.48 at 473 K. This model reproduced the experimental measurements almost perfectly. For PZT-0.48 and PZT-0.50 at 473 K, the composition ratio between *P*4*mm* and *Cm* was found to be approximately 3:1 and 4:1; for PZT-0.45 at 543 K, the *Cm* fraction is 37.1 (8)%, and this decreases to 29.1 (8)% at 623 K, which means *P*4*mm* is the major phase for all these three compositions and the concentration of *P*4*mm* increases with rising temperature.

4. Discussion

4.1. Tilt peaks

The main difference between the R_{LT} and R_{HT} phases in the old phase diagram (Jaffe *et al.*, 1971) is the octahedral tilt system. In the low-temperature and Zr-rich area, PZT has the tilt system $a^-a^-a^-$ which creates odd–odd–odd type reflections (with $k \neq l$, $h \neq l$, $h \neq k$) when expressed on a doubled pseudocubic unit cell (half indices on a pseudocubic unit cell; Glazer, 1972); while with temperature increasing or Zr concentration decreasing, the tilt peaks disappear gradually,

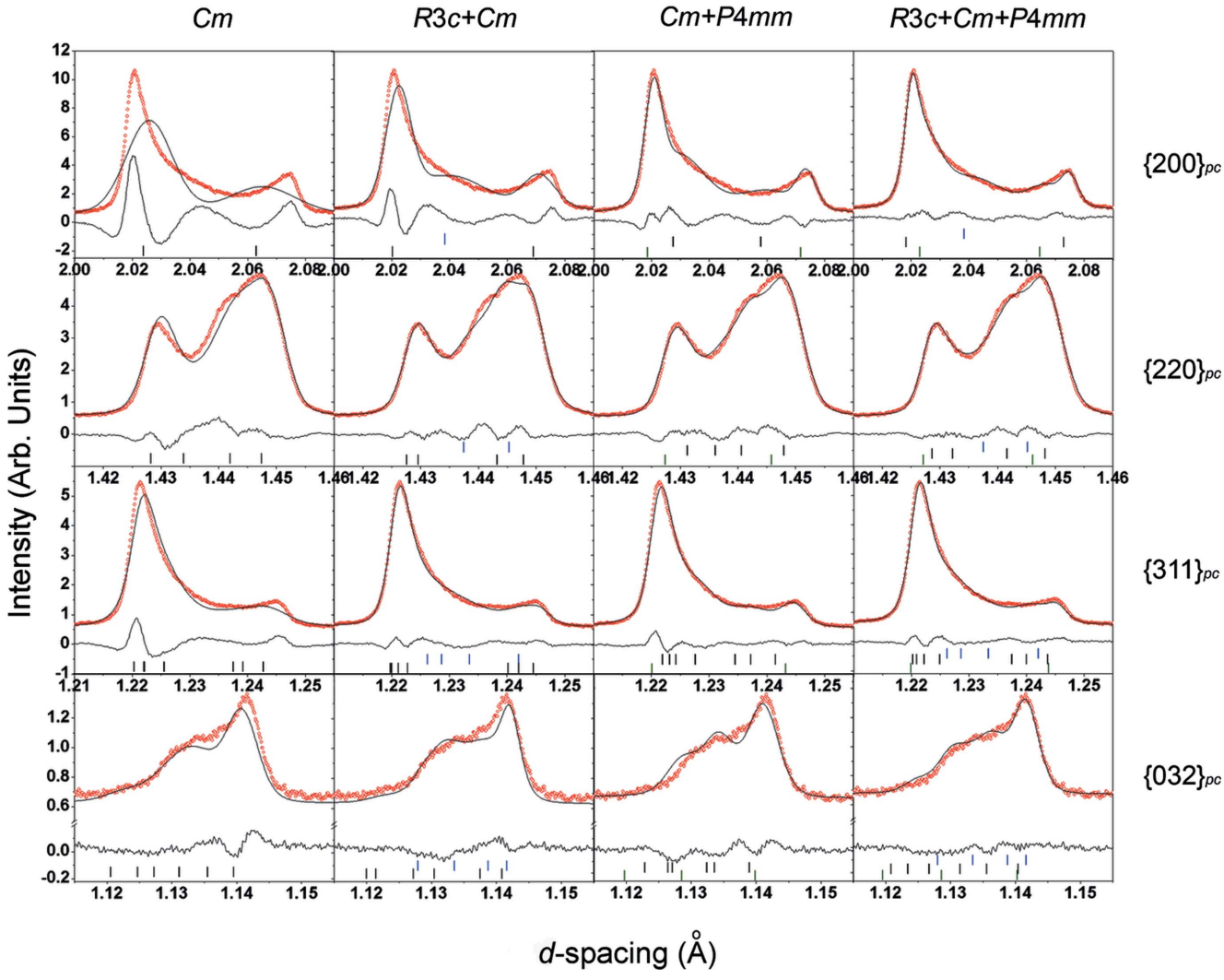

Figure 6
Refined profiles for $\{200\}_{pc}$, $\{220\}_{pc}$, $\{311\}_{pc}$ and $\{032\}_{pc}$ reflections for PZT-0.48 at 300 K with different refinement models.

indicating a phase change from a tilted system to a non-tilted $a^0a^0a^0$ system.

Our experiments showed the same trend. For PZT-0.3 several tilt peaks ($\{\frac{1}{2}\frac{3}{2}\frac{-3}{2}\}_{pc}$, $\{\frac{1}{2}\frac{5}{2}\frac{-1}{2}\}_{pc}$, $\{\frac{3}{2}\frac{5}{2}\frac{-5}{2}\}_{pc}$, $\{\frac{-1}{2}\frac{9}{2}\frac{-3}{2}\}_{pc}$, $\{\frac{5}{2}\frac{7}{2}\frac{-7}{2}\}_{pc}$, $\{\frac{5}{2}\frac{7}{2}\frac{-9}{2}\}_{pc}$ *etc.*) were observed at 10, 200 and 300 K, with the peak intensity decreasing as temperature increased: in the 473 K powder pattern, the tilt peaks no longer appear. At room temperature, compositions with $x \geq 0.4$ no longer show any observable tilt reflections. The low-temperature patterns at various compositions show a gradual disappearance of the oxygen tilts. Fig. 11 is the plot of the intensity of the $\{\frac{3}{2}\frac{5}{2}\frac{-5}{2}\}_{pc}$ reflection for PZT x = 0.30, 0.40, 0.45, 0.48 and 0.50 at around 10 K.

Hatch *et al.* (2002) refined PZT-0.48 at low temperature as a monoclinic tilted phase *Cc* partly based on the observation of the minus tilt reflections. However, as the $\{\frac{1}{2}\frac{1}{2}\frac{1}{2}\}_{pc}$ peak has never been observed by any experiments (Phelan *et al.*, 2010), the phase transition they proposed between high-temperature *Cm* and low-temperature *Cc* is more likely to be an R_{HT} and R_{LT} phase change with the existence of some other accompanying phases.

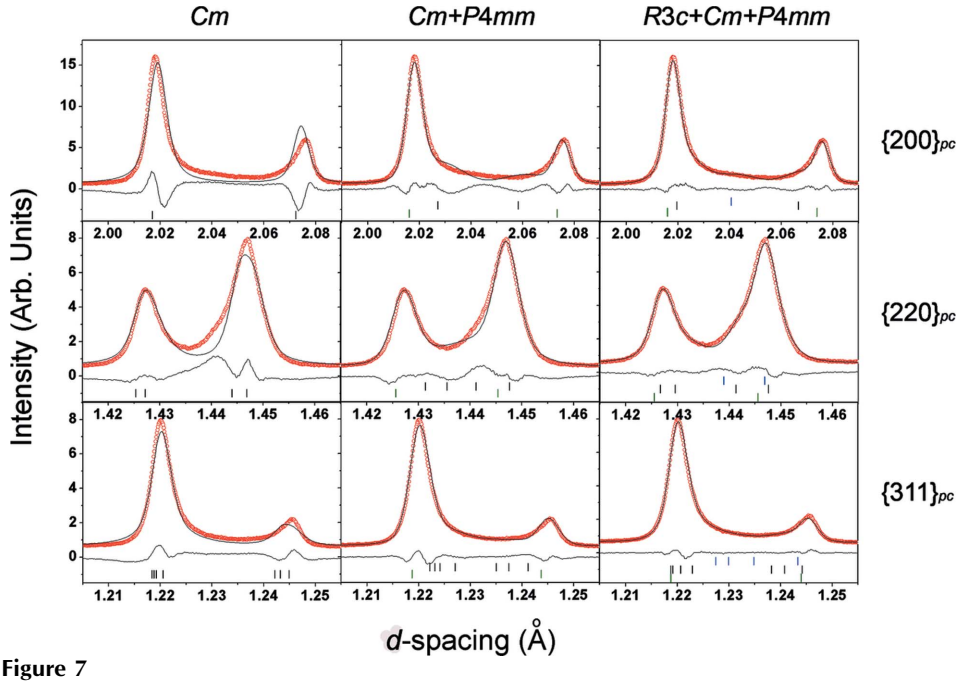

Figure 7
Refined profiles for $\{200\}_{pc}$, $\{220\}_{pc}$ and $\{311\}_{pc}$ reflections for PZT-0.5 at 300 K with different refinement models.

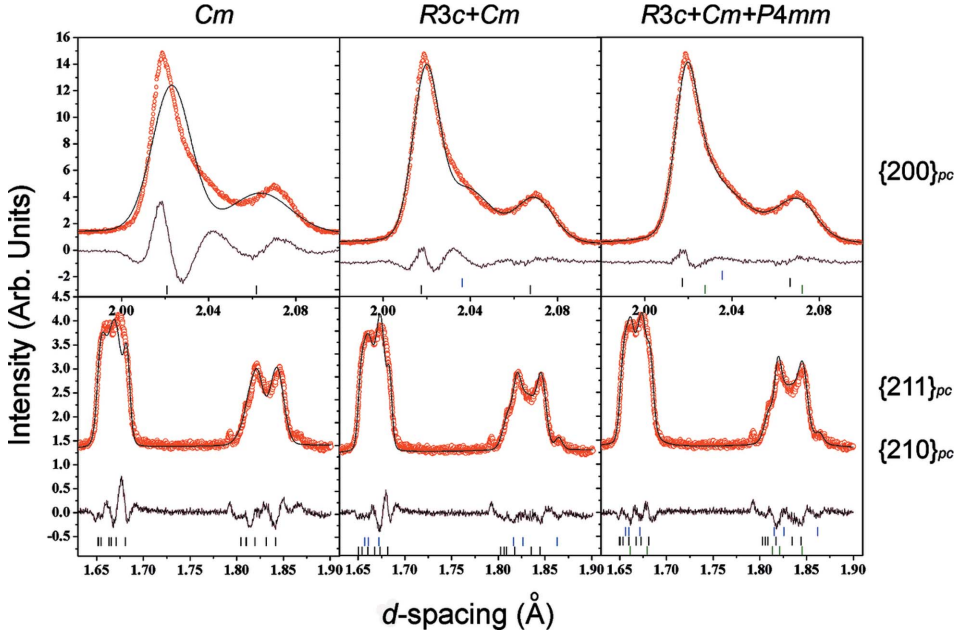

Figure 8
Refined profiles for $\{200\}_{pc}$ and $\{210\}_{pc}$ reflections for PZT-0.48 at 13 K with different refinement models.

In a single *R*3*c* phase, the intensities of the tilt reflections are directly related to the tilt angle ω, which can be calculated from the value of the rhombohedral structural parameter e [$\tan\omega = 4(3)^{1/2}e$; Megaw & Darlington, 1975]. However, in a mixed-phase model with *R*3*c* as the only tilted phase, the intensities of the tilt peaks are affected by both the values of the tilt angles and the quantity of the *R*3*c* phase present. The refinement results show a dramatic decrease of the *R*3*c* proportion from PZT-0.45 to PZT-0.48. Therefore, the refined e values for PZT-0.48 and PZT-0.50 are not very reliable. On the other hand, the PZT-0.30, PZT-0.40 and PZT-0.45 samples, which appear to contain approximately the same amount of *R*3*c* phase, display a relatively smooth decrease of ω [5.62 (1), 4.47 (2)° and 3.78 (2)°]. The sudden drop of the tilt peak intensity from PZT-0.45 to PZT-0.48 is consistent with the reduction of the amount of the *R*3*c* phase in the mixed-phase system.

4.2. Reliability of a 'real' monoclinic phase

As seen in the previous sections, the monoclinic *Cm* phase which was considered as a bridging phase in the MPB region by Noheda *et al.* (1999) is found across the whole region in our refinements. In order to examine the reliability of our multiphase models, the FWHM of $\{222\}_{pc}$ was plotted against x at 10 K (Fig. 12). This FWHM shows

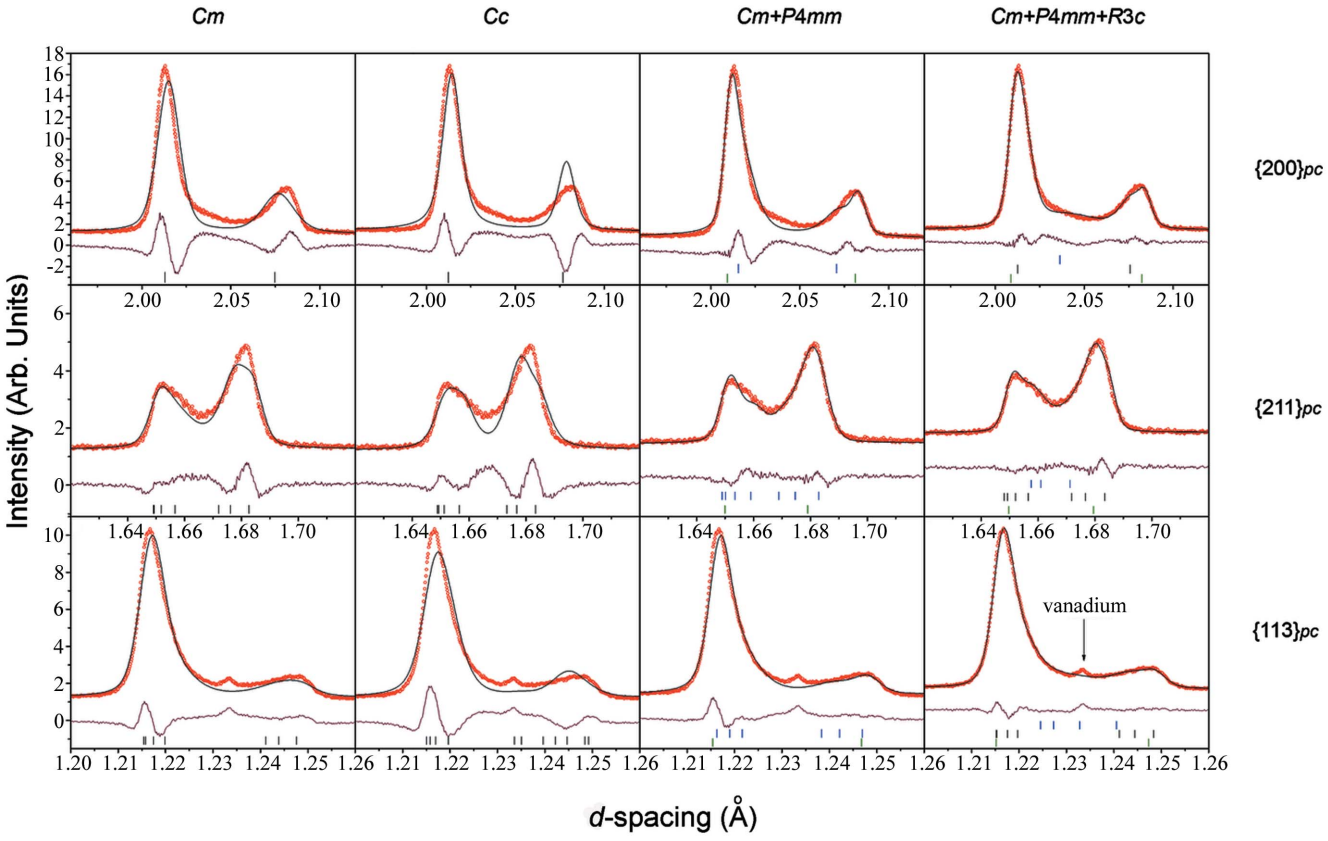

Figure 9
Refined profiles for $\{200\}_{pc}$, $\{211\}_{pc}$ and $\{113\}_{pc}$ reflections for PZT-0.5 at 10 K with different refinement models.

high correlation with the *Cm* fraction behaviour and suggests that the refinement of the *Cm* phase fraction derives mainly from peak broadening information, as opposed to the appearance of extra peaks. However, it is always possible that the peak broadening is caused by other reasons, including strain, particle size effects and domain-wall scattering *etc.*, and these possible causes must also be explored.

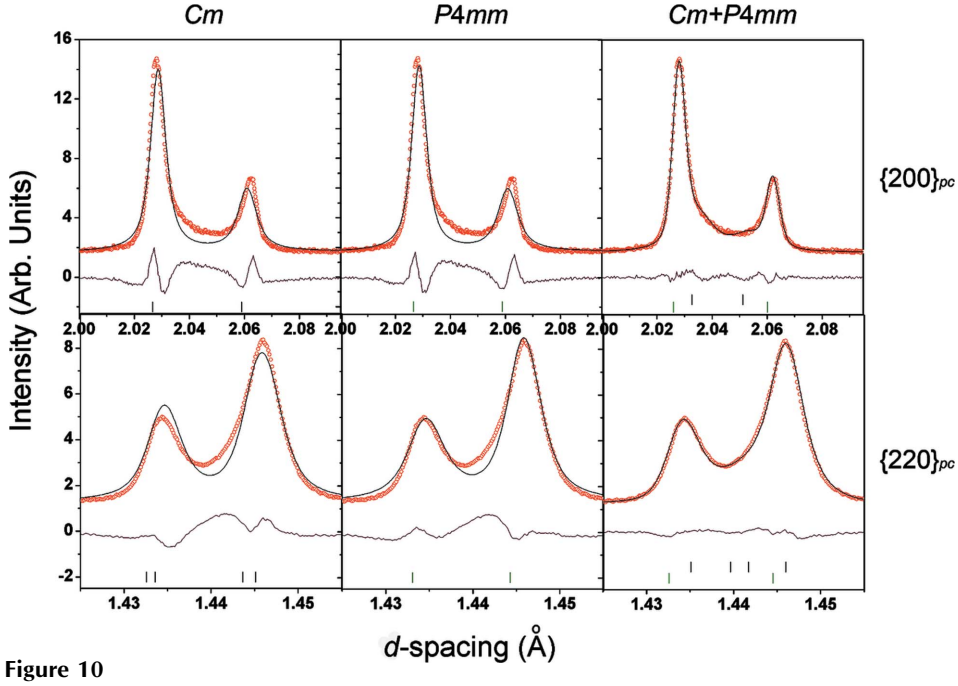

Figure 10
Refined profiles for $\{200\}_{pc}$ and $\{220\}_{pc}$ reflections for PZT-0.48 at 473 K with different refinement models.

The anisotropic strain effect was examined in the refinements, but this still showed that the multiphase model fits the data better. Wang (2006, 2007) investigated the diffraction effects caused by adaptive monoclinic phases (M_A/M_B phase for rhombohedral microdomains and M_C phase for tetragonal microdomains) with very low domain wall energy. This model was also examined with the PZT-0.6 and PZT-0.3/PZT-0.4 data. The lattice parameters of the M_C phase adapted from the tetragonal twin domain are in good agreement with the refined monoclinic *Pm* lattice parameters and the values of Wang's domain size coefficient *A*

are reasonable (at 10 K: A = 5.421; at 300 K: A = 5.536). However, the volume fractions of the twin layers ω at low temperature and room temperature are both much lower than the reported values for $Pb(Mg_{1/3}Nb_{2/3})_{1-x}Ti_xO_3$ and $Pb(Zn_{1/3}Nb_{2/3})_{1-x}Ti_xO_3$ in the MPB region (Wang, 2006; at 10 K: ω = 0.027; at 300 K: ω = 0.017 for PZT-0.6 in our case), which suggests that the amount of any adaptive phase present based on the observed monoclinic lattice parameters is comparatively very small, and does not appear to be of major significance in the observed data. On the rhombohedral side, Wang's (2007) calculation shows that the following identity should be true: $c_m = a_r = (a_m + b_m)/2(2)^{1/2}$. These three parameter values are plotted using our data in Fig. 13, where it can be seen that the equality of these parameters is not obeyed. The calculations in both tetragonal and rhombohedral twin domain cases suggest that in this material an adaptive monoclinic phase is not consistent with the unit-cell dimensions obtained from the refinements.

In addition, high-resolution X-ray single-crystal experiments on PZT-0.45 have shown extra diffracted intensity on reciprocal space maps that is not consistent with the domain-wall scattering (Gorfman *et al.*, 2011).

It would seem therefore that we have found no direct evidence for domain-wall scattering associated with adaptive phases, suggesting that the mixed-phase models, such as used here, are a better description of the PZT structures in the ceramics. However, we should add a note of caution here that in order to explain the peak profiles found in the diffraction data we are pushing the Rietveld method to its limits. The addition of every extra phase into the analysis means the introduction of more refineable fitting parameters. It is always possible that the introduction of other forms of extra scattering, such as from stacking faults (Schoenau & Leoni, 2010) may also explain the profile shapes, at least in the powders. On the other hand, the single-crystal measurements (Gorfman *et al.*, 2011) do seem to support the mixed-phase picture.

Further support for this comes from considering the refined phase fractions (expressed as percentages) as a function of x for different temperatures 10, 300 and 473 K, as shown in Fig. 14. Rietveld refinement of phase fractions, when the different structures are so closely related might be thought to be highly suspect. However, it can be seen that in each case the changes in the phase fractions do seem to follow the expected trends, suggesting that they are indeed meaningful.

This evidence shows that the *R*3*c*/*R*3*m* phase mainly exists in the Zr-rich region, especially at lower temperatures. It transforms into the *Cm* phase either with an increase in the temperature or with a decrease of the Zr content. In the Ti-rich region (PZT-0.6), *Cm* and *P*4*mm* phases coexist in almost

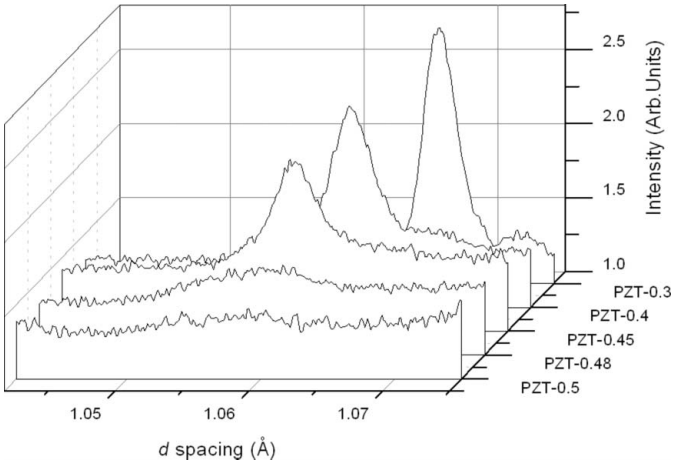

Figure 11
Intensity of the $\{\frac{3}{2}\frac{5}{2}\frac{-5}{2}\}_{pc}$ tilt reflection for PZT x = 0.30, 0.40, 0.45, 0.48 and 0.50 at around 10 K.

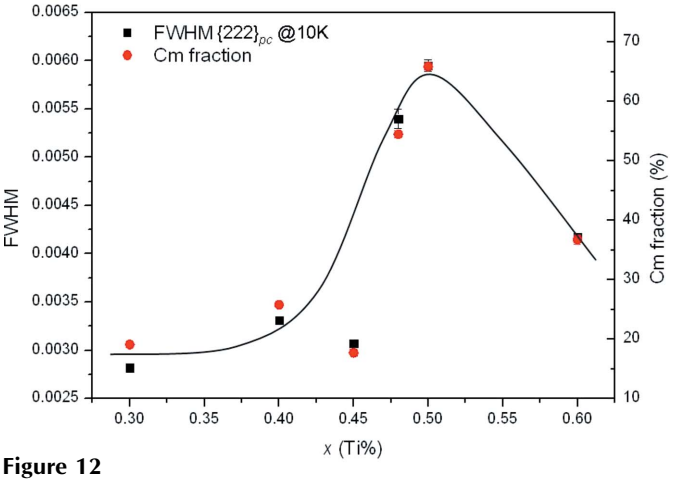

Figure 12
A comparison of the FWHM of the $\{222\}_{pc}$ reflections (red circles) and *Cm* fractions (black squares) against Ti concentrations at 10 K. The full line serves as a guide to the eye. This figure is in colour in the electronic version of this paper.

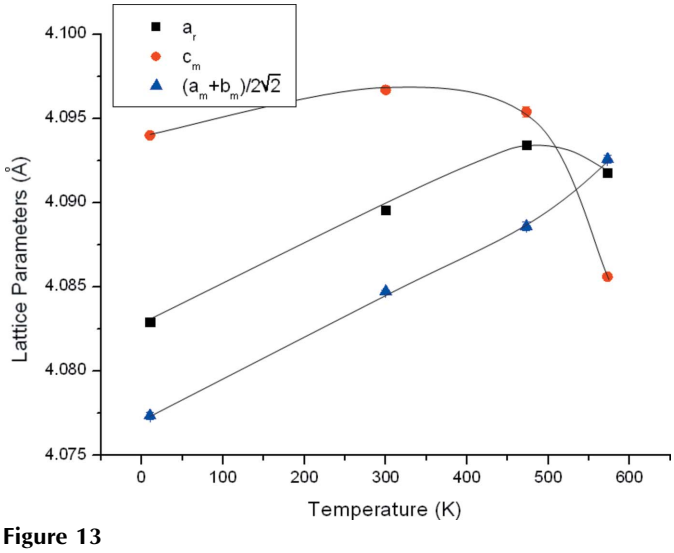

Figure 13
Temperature dependence of lattice parameters for PZT-0.4. Black squares: observed rhombohedral lattices; red circles: observed c for monoclinic; blue triangles: calculated $a_r = (a_m + b_m)/2(2)^{1/2}$ based on the adaptive phase model. This figure is in colour in the electronic version of this paper.

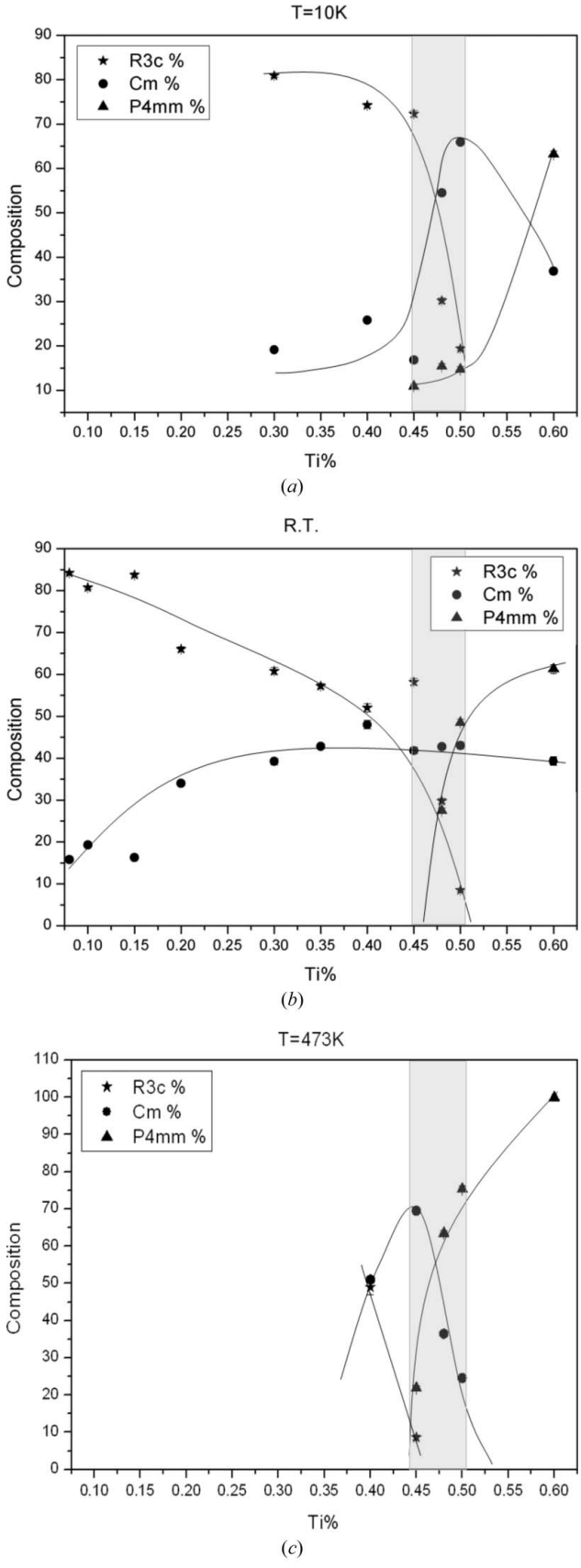

Figure 14
Plots of the phase fractions (percentages) with Ti concentration (x) at (a) 10 K, (b) 300 K and (c) 473 K. The grey shading indicates the MPB region.

the same amounts at low temperature. With increasing temperature, the amount of *Cm* decreases and at 473 K it disappears. In Fig. 15 the temperature dependence of the pseudocubic lattice constants for the refined *Cm* and *P4mm* phases is shown. Both lattice constants are similar and this result suggests that the *Cm* and *P4mm* structures are metrically interconvertible.

It is also instructive to plot contour maps of the refined *R3c*/*R3m* and *P4mm* fractions against temperature and composition (Figs. 16*a* and *b*). The data points are superimposed on the map, and the white lines describe the boundaries where the phase fractions change dramatically. They indicate more clearly that *R3c*/*R3m* exists mainly on the low-temperature Zr-rich side and *P4mm* on the high-temperature Ti-rich side with *Cm* as an accompaniment. The first-order phase transition between the major *R3c*/*R3m* and *P4mm* phases is seen as an inclined boundary more or less as reported for the MPB previously (Hinterstein *et al.*, 2010). However, the phase coexistences, especially at high temperature for PZT-0.45, have not been elucidated and described in previous studies.

The contour map for the *Cm* phase is shown in Fig. 16(*c*). Three phases coexist at low temperature, and the *Cm* phase is the major phase with small amounts of *R3c*/*R3m* and *P4mm* around $x = 0.5$. With increasing temperature, both *R3c*/*R3m* and *Cm* phase fractions decrease while the *P4mm* phase fraction increases. It is worth noticing that another area with a maximum *Cm* fraction is found around $x = 0.45$ at 550 K, and that both maximum areas coincide with where *R3c*/*R3m* tends to transform into the *P4mm* phase. Although the presence of the *Cm* phase is found over the whole compositional region, it plays a particularly important role in the MPB region in the way that *R3c*/*R3m* changes into *Cm* first and then the *Cm* phase transforms into *P4mm*.

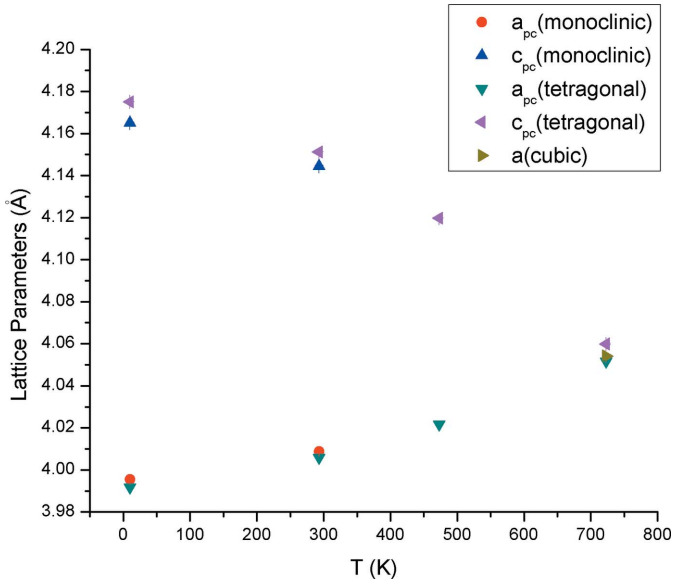

Figure 15
Temperature dependence of the pseudocubic lattice paramerters for PZT-0.6.

4.3. Construction of a new phase diagram

The contour maps of Fig. 16 seem to indicate good consistency in the refined values of the phase fractions and so this enables us to suggest a new phase diagram (Fig. 17) for the central region of the PZT composition range.

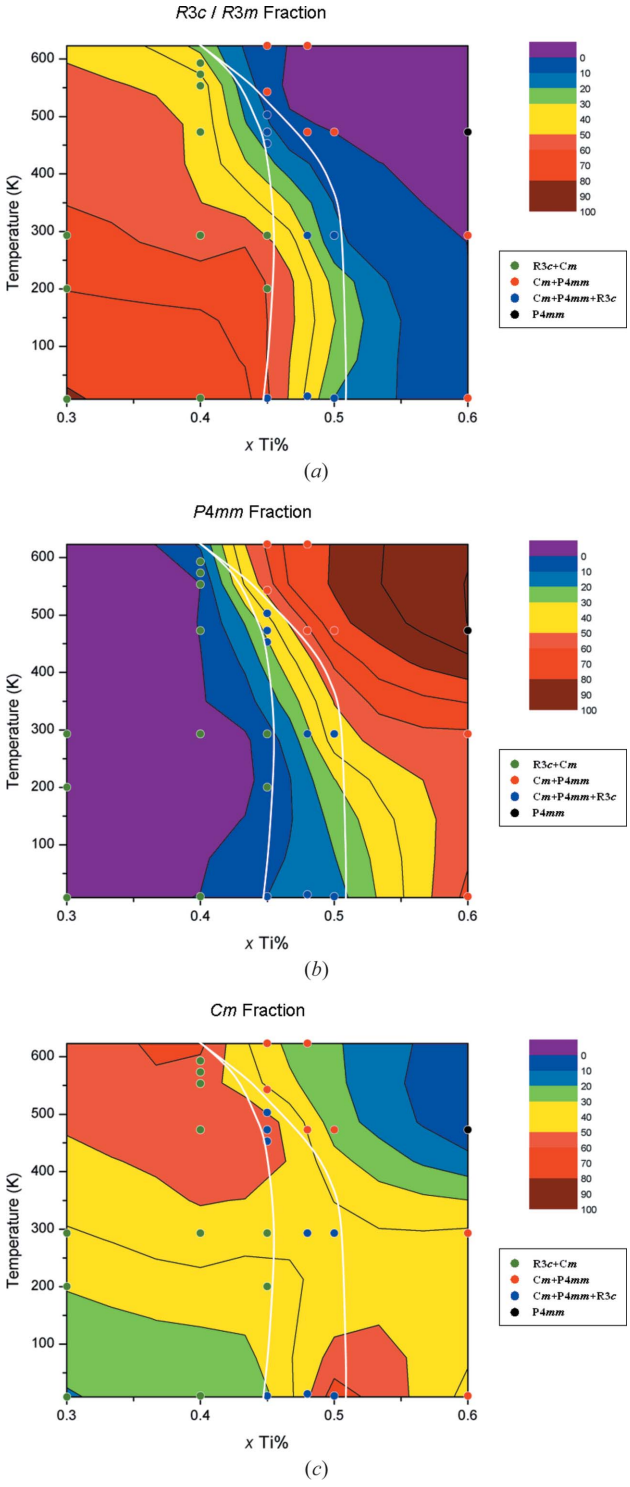

Figure 16
Contour maps for (*a*) *R*3*c*/*R*3*m*, (*b*) *P*4*mm* and (*c*) *Cm* phase fractions.

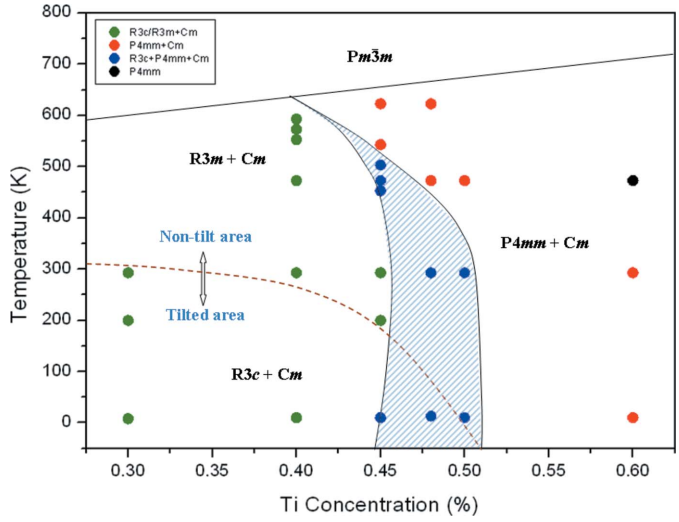

Figure 17
A new phase diagram for PZT ceramic with results for $0.30 \leq x \leq 0.6$ based on the neutron diffraction refinements.

Apart from the structural models we have proposed, which are different from the commonly accepted ones (Jaffe *et al.*, 1971; Noheda *et al.*, 1999), the shape of the MPB is seen to be steeply inclined at high temperature. The multi-phase nature of the ceramics, especially within and around the MPB region where there appear to be at least three phases present, means that there will be many phase boundaries and domain walls that can be moved and interchanged under applied stresses and electric fields, so that domain switching among rhombohedral, monoclinic and tetragonal states will be relatively easy, thus leading to enhanced piezoelectric properties, consistent with the idea of extrinsic contributions (Rogan *et al.*, 2003) being dominant.

5. Summary and conclusions

In this paper we have described Rietveld refinements for PZT over a large composition and temperature range ($0.3 \leq x \leq 0.6$, $8 \leq T \leq 623$ K). Several structural models were examined and the best are mixtures of rhombohedral and monoclinic symmetry on the Zr-rich side, tetragonal and monoclinic on the Ti-rich side, and three phases coexisting in the MPB region. In the refinements anisotropic strain broadening and domain-wall scattering effects were considered, but the inclusion of these did not alter the main conclusions. Since the refined values of the phase fractions seemed to follow physically sensible trends, a modified phase diagram for the central composition range of PZT is proposed.

We are grateful for financial support provided by EPSRC-NSF (Materials World Network: Nanoscale Structure-Property Relationships in Lead-free Morphotropic Phase Boundary Piezoelectrics). HY is grateful to the Grant-in-Aid for JSPS Fellows and the Global COE Program, 'Global Center of Excellence for Material System Innovation' by the

Ministry of Education, Culture, Sports, Science and Technology.

References

Asada, T. & Koyama, Y. (2004). *Phys. Rev. B*, **70**, 104105.
Asada, T. & Koyama, Y. (2007). *Phys. Rev. B*, **75**, 214111.
Bokov, A. A., Long, X. & Ye, Z.-G. (2010). *Phys. Rev. B*, **81**, 172103.
Boysen, H. (2005). *Z. Kristallogr.* **220**, 726–734.
Boysen, H. (2007). *J. Phys. Condens. Matter*, **19**, 275206.
Brown, I. D. (2002). *The Chemical Bond in Inorganic Chemistry: The Bond Valence Model.* Oxford University Press.
Coelho, A. A. (2005). *J. Appl. Cryst.* **38**, 455–461.
Corker, D. L., Glazer, A. M., Whatmore, R. W., Stallard, A. & Fauth, F. (1998). *J. Phys. Condens. Matter*, **10**, 6251–6269.
Cox, D. E., Noheda, B. & Shirane, G. (2005). *Phys. Rev. B*, **71**, 134110.
Frantti, J., Ivanov, S., Eriksson, S., Rundlof, H., Lantto, V., Lappalainen, J. & Kakihana, M. (2002). *Phys. Rev. B*, **66**, 064108.
Frantti, J., Lappalainen, J., Lantto, V., Nishio, S. & Kakihana, M. (1999). *J. Jpn. Appl. Phys.* **38**, 5679–5682.
Fraysse, G., Haines, J., Bornand, V., Rouquette, J., Pintard, M., Papet, P. & Hull, S. (2008). *Phys. Rev. B*, **77**, 064109.
Glazer, A. M. (1972). *Acta Cryst.* B**28**, 3384–3392.
Glazer, A. M., Mabud, S. A. & Clarke, R. (1978). *Acta Cryst.* B**34**, 1060–1065.
Gorfman, S., Keeble, D. S., Glazer, A. M., Long, X., Xie, Y., Ye, Z.-G., Collins, S. & Thomas, P. A. (2011). *Phys. Rev. B*, **84**, 020102.
Hatch, D. M., Stokes, H. T., Ranjan, R., Ragini, Mishra, S. K., Pandey, D. & Kennedy, B. J. (2002). *Phys. Rev.* B**65**, 212101.
Hinterstein, M., Schoenau, K. A., Kling, J., Fuess, H., Knapp, M., Kungl, H. & Hoffmann, M. J. (2010). *J. Appl. Phys.* **108**, 024110.
Jaffe, B., Cook, W. R. & Jaffe, H. (1971). *Piezoelectric Ceramics.* Academic Press: New York.
Jin, Y. M., Wang, Y., Khachaturyan, A. G., Li, J. F. & Viehland, D. (2003). *J. Appl. Phys.* **94**, 3629–3640.
Kornev, I. A., Bellaiche, L., Janolin, P. E., Dkhil, B. & Suard, E. (2006). *Phys. Rev. Lett.* **97**, 157601.
Kuroiwa, Y., Terado, Y., Kim, S. J., Sawada, A., Yamamura, Y., Aoyagi, S., Nishibori, E., Sakata, M. & Takata, M. (2005). *Jpn. J. Appl. Phys.* **44**, 7151–7155.
Liu, H., Harrison, R. & Putnis, A. (2001). *J. Appl. Phys.* **90**, 6321–6326.
Megaw, H. D. & Darlington, C. N. W. (1975). *Acta Cryst.* A**31**, 161–173.
Noheda, B., Cox, D. E., Shirane, G., Gonzalo, J. A., Cross, L. E. & Park, S.-E. (1999). *Appl. Phys. Lett.* **74**, 2059–2061.
Noheda, B., Cox, D. E., Shirane, G., Guo, R., Jones, B. & Cross, L. E. (2001). *Phys. Rev. B*, **63**, 014103.
Noheda, B., Gonzalo, J. A., Cross, L. E., Guo, R., Park, S.-E., Cox, D. E. & Shirane, G. (2000). *Phys. Rev. B*, **61**, 8687–8695.
Pandey, D., Singh, A. K. & Baik, S. (2008). *Acta Cryst.* A**64**, 192–203.
Phelan, D., Long, X., Xie, Y., Ye, Z. G., Glazer, A. M., Yokota, H., Thomas, P. A. & Gehring, P. M. (2010). *Phys. Rev. Lett.* **105**, 207601.
Ragini, Ranjan, R., Mishra, S. K. & Pandey, D. (2002). *J. Appl. Phys.* **92**, 3266–3274.
Rogan, R. C., Ustundag, E., Clausen, B. & Daymond, M. R. (2003). *J. Appl. Phys.* **93**, 4104–4111.
Sawaguchi, E. (1953). *J. Phys. Soc. Jpn*, **8**, 615–629.
Schoenau, K. A. & Leoni, M. (2010). Personal communication.
Stephens, P. W. (1999). *J. Appl. Cryst.* **32**, 281–289.
Theissmann, R., Schmitt, L. A., Kling, J., Schierholz, R., Schonau, K. A., Fuess, H., Knapp, M., Kungl, H. & Hoffmann, M. J. (2007). *J. Appl. Phys.* **102**, 024111.
Wang, Y. (2006). *Phys. Rev. B*, **73**, 014113.
Wang, Y. (2007). *Phys. Rev. B*, **76**, 024108.
Ye, Z.-G., Bokov, A. A., Xie, Y. & Long, X. (2010). ISAF-ECAPD 2010, Edinburgh, Abstract.
Yokota, H., Zhang, N., Taylor, A. E., Thomas, P. A. & Glazer, A. M. (2009). *Phys. Rev. B*, **80**, 104109.